One-sided Downward Control Chart for Monitoring the Multivariate Coefficient of Variation with VSSI Strategy

XinYing Chew[1] & Khai Wah Khaw[2*]

[1]School of Computer Sciences, Universiti Sains Malaysia, 11800 Pulau Pinang, Malaysia
[2]School of Management, Universiti Sains Malaysia, 11800 Pulau Pinang, Malaysia
*E-mail: khaiwah@usm.my

Abstract. In recent years, control charts monitoring the coefficient of variation (CV), denoted as the ratio of the variance to the mean, is attracting significant attention due to its ability to monitor processes in which the process mean and process variance are not independent of each other. However, very few studies have been done on charts to monitor downward process shifts, which is important since downward process shifts show process improvement. In view of the importance of today's competitive manufacturing environment, this paper proposes a one-sided chart to monitor the downward multivariate CV (MCV) with variable sample size and sampling interval (VSSI), i.e. the $VSSI_D$ MCV chart. This paper monitors the MCV as most industrial processes simultaneously monitor at least two or more quality characteristics, while the VSSI feature is incorporated, as it is shown that this feature brings about a significant improvement of the chart. A Markov chain approach was adopted for designing a performance measure of the proposed chart. The numerical comparison revealed that the proposed chart outperformed existing MCV charts. The implementation of the $VSSI_D$ MCV chart is illustrated with an example.

Keywords: *average time to signal; downward shifts; expected average time to signal; multivariate coefficient of variation; variable sample size and sampling interval.*

1 Introduction

Control charting is an important technique in Statistical Process Control (SPC). It is seen as an efficient process monitoring technique in various industries for detecting the presence of assignable causes, as can be seen from several research publications (see Djauhari [1], Chen, *et al.* [2], Wang [3], Chong, *et al.* [4]). In most real industry applications, it is common to deal with processes that monitor two, three or more quality characteristics. In this case, great attention is paid to multivariate process monitoring. Furthermore, when the process standard deviation is in line with the process mean, existing traditional charts that are used to monitor the process mean and process variance are unable to correctly detect the process signals. In this case it is suitable to use the coefficient of variation (CV). The CV is commonly used and its importance is

Received October 13th, 2019, 1st revision February 7th, 2020, Accepted for publication February 28th, 2020.
 ISSN: 2337-5760,
DOI: 10.5614/j.math.fund.sci.2020.52.1.8

shown through applications in many disciplines. Singh & Singh [5] used CV to investigate video frame and region duplication forgery detection. Salmanpour, *et al.* [6] applied CV to resolve the robot path-planning problem with multiple objectives. Lengler & Steger [7] studied the CV of neuronal spike trains and Zhou, *et al.* [8] suggested a G1-CV approach for the best development face ventilation mode selection. The application of CV in chatter detection [9] and spectrophotometric repeatability measurement [10] have also been discussed. Ushigome, *et al.* [11] and Romano, *et al.* [12] investigated the CV of home blood pressure and shear and tensile strength experiments, respectively.

Kang, *et al.* [13] were the first researchers to introduce a standard CV control chart. In the last decade, numerous CV charts have been proposed to increase the effectiveness of existing standard CV charts for detecting CV shifts, such as those by Khaw, *et al.* [14], Yeong, *et al.* [15], Khaw & Chew [16], Lim, *et al.* [17], etc. Conversely, Yeong, *et al.* [18] introduced two one-sided multivariate CV (MCV) charts (SH MCV) to fill the research gap related to the multivariate process. Khaw, *et al.* [19,20] discussed adaptive MCV and synthetic MCV charts to increase the statistical performance of the SH MCV chart of Yeong, *et al.* [18]. Later, run rules and variable parameter MCV charts were introduced [21,22]. More recently, an exponentially weighted moving average (EWMA) MCV chart was recommended by Giner-Bosch, *et al.* [23], whereas Haq & Khoo [24] considered an adaptive EWMA MCV chart.

Meanwhile, adaptive control charting methods are known to be practical when compared to non-adaptive charts (Epprecht, *et al.* [25], Deheshvar, *et al.* [26]). From the existing adaptive schemes, the variable sample size and sampling interval (VSSI) scheme is one of the best adaptive schemes. After the VSSI $\bar{X}$ chart [27] was developed, the VSSI scheme was extended to various types of control charts. For example, Saha, *et al.* [28] developed an auxiliary information based VSSI chart to monitor the process mean. Kosztyan & Katona [29] and Khoo, *et al.* [30] applied risk-based VSSI and $VSSI_t$ S control charts, respectively. A VSSI median chart with measurement errors and estimated parameters have been suggested by Cheng & Wang [31].

The VSSI MCV chart [19] has superior performance in the detection of MCV shifts when compared to other existing MCV charts. However, a downside of this method is that the VSSI MCV chart was developed only for detecting upward MCV shifts. In most scenarios, the detection of downward MCV shifts is crucial since they show process improvement. With the intention to fill the research gap related to downward process monitoring and the excellent features of the VSSI scheme, this paper extends the VSSI MCV chart of Khaw, *et al.* [19] and proposes a one-sided downward VSSI ($VSSI_D$) chart for monitoring downward MCV shifts. Note that the one-sided VSSI_D MCV chart can avoid biased average time to signal (ATS) performance. The VSSI scheme in Aparisi & Haro [32] was adopted to design the VSSI_D MCV chart. The VSSI_D MCV chart gives the flexibility for practitioner to vary sample size n and sampling interval h. The VSSI_D MCV chart is expected to surpass the existing SH_D MCV chart.

Hereafter, Section 2 illustrates the fundamental properties of the SH_D MCV chart. Section 3 describes the details of the VSSI_D MCV chart. The performance measures were evaluated using the Markov chain method. Performance comparisons of the existing VSSI_D MCV charts in terms of the ATS and expected average time of signal (EATS) criteria are discussed in Section 4. In Section 5, the new method's implementation is illustrated with an example. In the last section, the research findings and future recommendations are given.

2 The Downward SH MCV (SH_D MCV) Chart

Let $\boldsymbol{X}_1, \boldsymbol{X}_2, \dots, \boldsymbol{X}_n$ refer to a multivariate n_0 from the p-variate normal distribution with μ and Σ. Here, μ is the mean vector while Σ denotes the covariance matrix. Then, the MCV population statistics are denoted as

$$\gamma = (\mu^T \sum{}^{-1} \mu)^{-\frac{1}{2}} \tag{1}$$

[33]. The sample MCV, $\hat{\gamma}$, is used for estimating γ when μ and Σ are unknown. To derive $\hat{\gamma}$ from Eq. (1), $\bar{\boldsymbol{X}}$ and $\boldsymbol{S}$ should be computed so that they can replace μ and Σ, as follows:

$$\bar{\boldsymbol{X}} = \frac{1}{n_0} \sum_{i=1}^{n} \boldsymbol{X}_i \tag{2}$$

and

$$\boldsymbol{S} = \frac{1}{n_0 - 1} \sum_{i=1}^{n} \left(\boldsymbol{X}_i - \bar{\boldsymbol{X}}\right)\left(\boldsymbol{X}_i - \bar{\boldsymbol{X}}\right)^T \tag{3}$$

respectively. $\bar{\boldsymbol{X}}$ denotes the sample mean while $\boldsymbol{S}$ is a sample covariance matrix and they are independent. Hence, $\hat{\gamma}$ is obtained as

$$\hat{\gamma} = \left(\bar{\boldsymbol{X}}^T \boldsymbol{S}^{-1} \bar{\boldsymbol{X}}\right)^{-\frac{1}{2}} \tag{4}$$

A chart is set up by using the Phase-I data. If the target in-control MCV, γ_0 is unknown, then it can be estimated from the in-control $\hat{\gamma}_0$, which can be assumed from the Phase-I data. Note that $\hat{\gamma}_0$ is computed based on the root mean square estimator

$$\hat{\gamma}_0 = \sqrt{\frac{1}{m}\sum_{i=1}^{m}\hat{\gamma}_i^2} \tag{5}$$

where m and $\hat{\gamma}_i^2$ are defined as the number of in-control multivariate samples from the Phase-I data used to estimate γ_0 and the squared i-th Phase-I sample MCV (for i = 1, 2, …, m), respectively.

The cumulative distribution function (cdf) of the $\hat{\gamma}$ is derived as [18]

$$F_{\hat{\gamma}}\left(x \middle| n_0, p, \delta\right) = 1 - F_F\left(\frac{n_0(n_0 - p)}{(n_0 - 1)px^2}\middle| p, n_0 - p, \delta\right), \tag{6}$$

where $F_F(\cdot)$ refers to the cdf of a non-central F distribution, together with p and $n_0 - p$ degrees of freedom and non-centrality parameter δ, where p denotes the number of quality characteristics, where Eq. (6) can be only considered valid when $n_0 > p$ as the degree of freedom for the non-central F distribution must be positive. The non-centrality parameter is obtained as $\delta = \frac{n_0}{(\tau_\gamma)^2}$, where the shift size $\tau = 1$ (in-control process). The out-of-control MCV is computed as $\gamma_1 = \tau\gamma_0$, where $\tau \neq 1$. Consequently, the inverse cdf of $\hat{\gamma}$ is [18]

$$F_{\hat{\gamma}}^{-1}\left(\alpha \middle| n_0, p, \delta\right) = \sqrt{\frac{n_0(n_0 - p)}{(n_0 - 1)p}\left[\frac{1}{F_F^{-1}\left(1 - \alpha \middle| p, n_0 - p, \delta\right)}\right]}, \tag{7}$$

where $F_F^{-1}(\cdot)$ refers to the inverse cdf of a non-central F distribution with p and $n_0 - p$ degrees of freedom and non-centrality parameter δ.

Since the distribution of $\hat{\gamma}$ is skewed, the one-sided downward SH MCV chart for the downward MCV shifts is suggested [18]. Here, the SH$_D$ MCV chart contains the lower control limit (LCL). The LCL of the SH$_D$ MCV chart is specified with the Type-I error probability α. Then, the LCL can be obtained as

$$\text{LCL} = F_{\hat{\gamma}}^{-1}\left(\alpha \mid n_0, p, \delta_0\right), \tag{8}$$

where $\delta_0 = \frac{n_0}{\gamma_0^2}$ [18]. The probability for the SH$_D$ MCV chart for an out-of-control signal detection is given as $A = \Pr(\hat{\gamma} < \text{LCL})$.

The performance measures for the SH_D MCV chart were adopted from Yeong, *et al.* [18]. Thus, the average run length (ARL) and out-of-control expected average run length ($EARL_1$) of the SH_D MCV charts can be obtained as

$$\text{ARL}=\frac{1}{A} \tag{9a}$$

and

$$\text{EARL}_1=\int_{\tau_{\min}}^{\tau_{\max}} \text{ARL}_1\left(\text{LCL}, I, n_0, \gamma_0, \tau\right) f_\tau\left(\tau\right) d\tau \tag{9b}$$

Note that $\delta_1 = \frac{n_0}{(\tau\gamma_0)^2}$, where $\tau \neq 1$. Here, $\tau = 1$ will results in in-control ARL (ARL_0) while $\tau \neq 1$ results in out-of-control ARL (ARL_1). When $\tau \neq 1$, the values of $0 < \tau < 1$ correspond to downward MCV shifts, respectively. For the $EARL_1$ computation using Eq. (9b), the in-control EARL ($EARL_0$) is set to be equal to ARL_0 and $f_\tau(\tau)$ is the probability density function (pdf) of τ. Additionally, τ_{min} and τ_{max} are the lower and upper bounds of τ, respectively.

3 The Downward VSSI MCV ($VSSI_D$ MCV) Chart

The existing SH_D MCV chart has a static sample size, n_0 and sampling interval, h_0. This chart consists of two regions and a border, i.e. the central and action regions with LCL. Different from the SH_D MCV chart, the $VSSI_D$ MCV chart contains three regions and two borders, i.e. the central, warning and action regions, with a lower warning limit (LWL) and LCL. The VSSI scheme can vary n_0 and h_0 to enhance the sensitivity of the SH_D MCV chart for detecting small and moderate downward shifts. The sample size of the proposed chart can be differentiated between a small and large sample size, i.e. n_1 and n_2, where $n_1 < ASS_0 < n_2$ while the sampling interval can be differentiated between short and long sampling intervals, i.e. h_1 and h_2, where $h_1 < ASI_0 < h_2$. Note that ASS_0 denotes the in-control average sample size whereas ASI_0 refers to the in-control average sampling interval, where $\text{ASS}_0$and ASI_0 of the $VSSI_D$ MCV chart are equal to those of n_0 and h_0 of the SH_D MCV chart for a fair statistical comparison. The $VSSI_D$ MCV chart works as follows (Figure 1):

1. When the *i*-th sample MCV, $\hat{\gamma}_i$ plots in the central region, then the process is said to be in-control and no further action is required. Hence, n_1 and h_2 should be used to obtain the next sample MCV, $\hat{\gamma}_{i+1}$.
2. When $\hat{\gamma}_i$ plots in the warning region, then the process is said to be still in-control. However, there is a high possibility for it to go out-of-control. Hence, n_2 and h_1 should be used to compute $\hat{\gamma}_{i+1}$.

3. When $\hat{\gamma}_i$ falls in the action region, the process is said to be out-of-control because of the presence of assignable causes. In this case, the practitioner should take corrective actions.

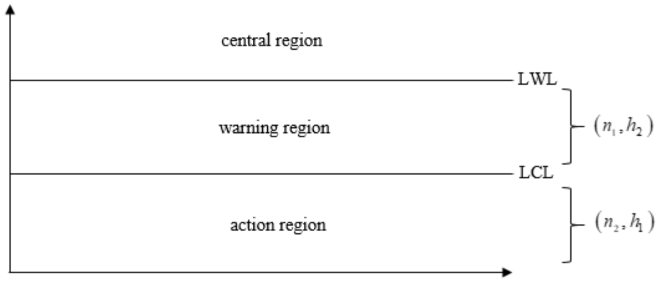

Figure 1 Graphical view of the VSSI$_D$ MCV chart.

In this paper, the lower control limit of the VSSI$_D$ MCV chart can be computed using Eq. (8), while the LWL is expressed as follows:

$$\mathrm{LWL} = F_{\hat{\gamma}}^{-1}\left(\alpha' \mid n_0, p, \delta_0\right) \tag{10}$$

where $F_{\hat{\gamma}}^{-1}(\cdot \mid n_0, p, \delta_0)$ is the inverse CDF of $\hat{\gamma}$ and $\delta_0 = \frac{n_0}{\gamma_0^2}$. Here, the α' value is determined to satisfy the desired ATS$_0$ value based on the in-control process MCV and $\alpha' > \alpha$.

The Markov chain approach was developed for the formula derivation of the ATS of the VSSID MCV chart. ATS is defined as the average amount of time for an out-of-control signal detection from time of a process shift occurrence. Here, the Markov-chain model of the VSSID MCV chart contains three states, i.e. the central, warning and action region. States 1 to 2 and 3 denote the transient states and absorbing state, respectively, as:

State 1: $\hat{\gamma} \in [\mathrm{LWL}, +\infty]$
State 2: $\hat{\gamma} \in (\mathrm{LCL}, \mathrm{LWL}]$
State 3: $\hat{\gamma} \in (0, \mathrm{LCL})$.

The transition probabilities matrix (tpm), given a change τ is given as:

$$\boldsymbol{P}^{\tau} = \begin{pmatrix} P_{11}^{\tau} & P_{12}^{\tau} & P_{13}^{\tau} \\ P_{21}^{\tau} & P_{22}^{\tau} & P_{23}^{\tau} \\ P_{31}^{\tau} & P_{32}^{\tau} & P_{33}^{\tau} \end{pmatrix}, \tag{11}$$

where P_{jk}^{τ} refers to the transition probability, which can be seen from the previous state j to the current state k, when the MCV has a shift change τ. The transient states in matrix $\boldsymbol{P}^{\tau}$ in Eq. (11) are listed as follows:

$$P_{11}^{\tau} = \Pr\left(\hat{\gamma} \geq \mathrm{LWL} \middle| n_1, p, \delta_{11}\right) = 1 - F_{\hat{\gamma}}\left(\mathrm{LWL} \middle| n_1, p, \delta_{11}\right)$$

$$P_{12}^{\tau} = \Pr\left(\mathrm{LCL} < \hat{\gamma} \leq \mathrm{LWL} \middle| n_1, p, \delta_{11}\right) \tag{12a}$$

$$= F_{\hat{\gamma}}\left(\mathrm{LWL} \middle| n_1, p, \delta_{11}\right) - F_{\hat{\gamma}}\left(\mathrm{LCL} \middle| n_1, p, \delta_{11}\right) \tag{12b}$$

$$P_{21}^{\tau} = \Pr\left(\hat{\gamma} \geq \mathrm{LWL} \middle| n_2, p, \delta_{12}\right) = 1 - F_{\hat{\gamma}}\left(\mathrm{LWL} \middle| n_2, p, \delta_{12}\right)$$

$$P_{22}^{\tau} = \Pr\left(\mathrm{LCL} < \hat{\gamma} \leq \mathrm{LWL} \middle| n_2, p, \delta_{12}\right) \tag{12c}$$

$$= F_{\hat{\gamma}}\left(\mathrm{LWL} \middle| n_2, p, \delta_{12}\right) - F_{\hat{\gamma}}\left(\mathrm{LCL} \middle| n_2, p, \delta_{12}\right) \tag{12d}$$

Subsequently, the ATS of the $\mathrm{VSSI_D}$ MCV charts can be computed as

$$\mathrm{ATS} = \boldsymbol{b}^T \left(\boldsymbol{I} - \boldsymbol{Q}\right)^{-1} \boldsymbol{t} \tag{13}$$

$\boldsymbol{I}$ and $\boldsymbol{Q}$ are the identity and transient state transition probability matrices with 2×2 dimension, respectively, whereas $\boldsymbol{t}^T = (h_2, h_1)$ is a sampling intervals vector. Subsequently, $\boldsymbol{b}^T = (b_1, b_2)$ represents the initial probability vector, satisfying $b_1 + b_2 = 1$. Here, b_1 and b_2 are the time spent proportions in the central and warning regions, respectively. Both b_1 and b_2 are obtained based on $\tau = 1$, where

$$b_1 = \frac{1 - F_{\hat{\gamma}}\left(\mathrm{LWL} \middle| n_1, p, \delta_{11}\right)}{1 - F_{\hat{\gamma}}\left(\mathrm{LCL} \middle| n_1, p, \delta_{11}\right)} \tag{14a}$$

$$b_2 = \frac{F_{\hat{\gamma}}\left(\mathrm{LWL} \middle| n_2, p, \delta_{12}\right) - F_{\hat{\gamma}}\left(\mathrm{LCL} \middle| n_2, p, \delta_{12}\right)}{1 - F_{\hat{\gamma}}\left(\mathrm{LCL} \middle| n_2, p, \delta_{12}\right)} \tag{14b}$$

subject to the specified values of $\mathrm{ASS_0}$ and $\mathrm{ASI_0}$, where

$$\mathrm{ASS_0} = n_1 b_1 + n_2 b_2 \tag{15a}$$

$$\mathrm{ASI_0} = h_2 b_1 + h_1 b_2 \tag{15b}$$

Generally, τ must be specified when computing the ATS. The EATS can be applied to measure the chart's performance when the exact value of τ cannot be specified [19]. The in-control EATS ($\mathrm{EATS_0}$) value of the $\mathrm{VSSI_D}$ MCV chart is set as $\mathrm{ATS_0}$ value and the $\mathrm{EATS_1}$ value is obtained as

$$\mathrm{EATS_1} = \int_{\tau_{\min}}^{\tau_{\max}} \mathrm{ATS_1}\left(\mathrm{LCL}, \mathrm{LWL}, n_1, n_2, h_1, h_2, \alpha, \alpha', \gamma_0, \tau\right) f_{\tau}\left(\tau\right) d\tau, \tag{16}$$

The actual shape of $f_\tau(\tau)$ is hard to be fitted if there is no information on $f_\tau(\tau)$. In this circumstance, τ can be assumed to follow a uniform distribution over the interval (τ_{min}, τ_{max}). This distribution was adopted by most researchers, i.e. Chong, *et al.* [34], Khaw, *et al.* [19], etc. Here, a uniform distribution can be used if the random variable is uncertain, excluding its upper and lower bounds [35]. Castagliola, *et al.* [36] have suggested the interval $(\tau_{min}, \tau_{max}) = [0.5,1)$ for the downward EWMA CV^2 chart.

The optimization procedure to compute the optimal parameter combinations (n_1, n_2, h_2, α') of the VSSI$_D$ MCV chart for minimizing the ATS_1 and $EATS_1$ values for detecting downward MCV shifts, τ and shift interval (τ_{min}, τ_{max}) were considered in this study. Note that h_1 is set as 0.1 and $ATS_0 = 370$. The α' parameter is used to obtain the LWL of the VSSI$_D$ MCV chart using Eq. (10). The application of the optimization procedure is for

1. $\text{Min}_{\{n_1,n_2,h_2,\alpha'\}}\text{ATS}_1(\tau)$, subject to constraint $ATS_0 = 370$, $\text{ASS}_0 = n_0$ and $\text{ASI}_0 = h_0$,
2. $\text{Min}_{\{n_1,n_2,h_2,\alpha'\}}\text{E}ATS_1(\tau_{min}, \tau_{max})$, subject to constraint $EATS_0 = 370$, $\text{ASS}_0 = n_0$ and $\text{ASI}_0 = h_0$.

Subsequently, the procedure of optimization of the VSSI$_D$ MCV chart is given as

Step 1: Specify n_0, h_0, h_1, p, τ (for $\text{ATS}_1(\tau)$) or (τ_{min}, τ_{max}) (for $\text{E}ATS_1(\tau_{min}, \tau_{max})$.

Step 2: Let $n_1 = p + 1$ and $n_2 = n_0 + 1$.

Step 3: Compute α using nonlinear equation solver, subject to constraint ATS_0=370. Then compute α' and h_2 using Eq. (17) and Eq. (18) listed as follows:

$$\alpha' = 1 - \frac{(n_2 - n_0)[1 - F_{\hat{\gamma}}(\text{LCL}|n_0, p, \delta_0)] + n_0 - n_1}{n_2 - n_1}, \tag{17}$$

and

$$h_2 = \frac{h_0(n_2 - n_1) - h_1(n_0 - n_1)}{n_2 - n_0}. \tag{18}$$

Step 4: Compute $\text{ATS}_1(\tau)$ value (or $\text{E}ATS_1(\tau_{min}, \tau_{max})$ value) using Eq. (13) (or Eq. (16)) with the optimal parameter combination (n_1, n_2, h_2, α') obtained from Steps 1 to 3.

Step 5: Let $n_1 + 1$ while retaining the same value of n_2.

Step 6: Repeat steps 3 to 5 until $n_1 = n_0 - 1$.

Step 7: Reset n_1 to $p + 1$ and let $n_2 + 1$.

Step 8: Repeat steps 3 to 7 until $n_2 = 31$. Here, $n_2 = 31$ can be viewed as a guideline. The practitioner will decide the maximum value of the sample size by depending on the characteristics of the process.

Step 9: Identify and select the parameter combination (n_1, n_2, h_2, α') that minimizes the $\mathrm{ATS}_1(\tau)$ value (or $EATS_1(\tau_{min}, \tau_{max})$ value) as the optimal parameter (n_1, n_2, h_2, α') combination.

4 Numerical Comparison

The existing $\mathrm{SH_D}$ MCV chart has $h_0 = 1$. Since ATS $= h_0 \times$ ARL, then ATS = ARL for the $\mathrm{SH_D}$ MCV chart. For a fair performance comparison with the existing $\mathrm{SH_D}$ MCV chart, the $\mathrm{ASI}_0 (= h_0)$ of the $\mathrm{VSSI_D}$ MCV chart is specified as unity. In this study, the (n_1, n_2) parameter combinations were varied to minimize the ATS_1 value, for detecting downward MCV shifts subject to constraints $3 \leq n_1 < n_0 \leq n_2 \leq 31$ and $4 \leq n_1 < n_0 \leq n_2 \leq 31$, for $p = 2$ and 3, respectively, where $n_0 = 5$ and 10 were considered. Note that these constraints were adopted from Yeong, *et al.* [18] and Khaw, *et al.* [19]. Thus, the computed $(n_1, n_2, h_1, h_2, \alpha, \alpha')$ parameter combinations using the aforementioned optimization procedure were varied to minimize the ATS_1 and EATS_1 values, for detecting downward MCV shifts, $\tau \in \{0.5, 0.6, 0.7, 0.8, 0.9\}$ and $(\tau_{max}, \tau_{min}) \in [0.5,1)$, where $p \in \{2,3\}$, $n_0 \in \{5,10\}$ and $\gamma_0 \in \{0.1, 0.3, 0.5\}$. We assume $\mathrm{ATS}_0 = 370$.

Table 1 presents the optimal parameter (n_1, n_2, h_2, α') combinations of the $\mathrm{VSSI_D}$ MCV chart that minimize the ATS_1 and EATS_1 values, for $\tau \in \{0.5, 0.6, 0.7, 0.8, 0.9\}$ and $(\tau_{max}, \tau_{min}) \in [0.5,1)$, where $p \in \{2,3\}$, $n_0 \in \{5,10\}$ and $\gamma_0 \in \{0.1, 0.3, 0.5\}$. For example, from Table 1, to minimize the ATS_1 value for detecting downward MCV shift $\tau = 0.5$, when $p = 2$, $n_0 = 5$, $h_1 = 0.1$ and $\gamma_0 = 0.1$, the optimal parameter combination (n_1, n_2, h_2, α') is 3, 10, 1.360 and 0.2876. These optimal parameter combinations presented in Table 1 were used to compute the ATS_1 and EATS_1 values for the $\mathrm{VSSI_D}$ MCV chart in Table 2. Table 2 presents the ATS_1 and EATS_1 values for the $\mathrm{VSSI_D}$ MCV and $\mathrm{SH_D}$ MCV charts [18], for $\tau \in \{0.5, 0.6, 0.7, 0.8, 0.9\}$ and $(\tau_{max}, \tau_{min}) \in [0.5,1)$, where $p \in \{2,3\}$, $n_0 \in \{5,10\}$ and $\gamma_0 \in \{0.1, 0.3, 0.5\}$. In order to show the superior performance of the proposed chart, the downward variable sampling interval (VSI) and variable sample size (VSS) charts were included in the performance comparison by letting $n_1 = n_2 = n_0$ and $h_1 = h_2 = h_0$, respectively. The VSSI$_D$ MCV chart outperformed the VSI$_D$ MCV, VSS$_D$ MCV and SH$_D$ MCV [18] charts, for detecting downward MCV shifts in terms of the ATS$_1$ and EATS$_1$ criteria. For instance, in Table 2, when $p = 2$, $n_0 = 5$, $\gamma_0 = 0.3$ and $\tau = 0.7$, the VSSI$_D$ MCV, VSI$_D$ MCV, VSS$_D$ MCV and SH$_D$ MCV charts yielded ATS$_1$ = 15.68, 33.33, 18.12 and 135.30, respectively. Another example can be shown from Table 3, when $p = 3$, $n_0 = 10$, $\gamma_0 = 0.1$ and $(\tau_{max}, \tau_{min}) = [0.5,1)$, the VSSI$_D$ MCV, VSI$_D$ MCV, VSS$_D$ MCV and SH$_D$ MCV charts yielded EATS$_1$ = 57.47, 61.74, 71.82 and 203.86, respectively. The results show that the VSSI$_D$ MCV charts yielded the best ATS$_1$ and EATS$_1$ values to detect small and moderate downward MCV shifts.

5 Example

The implementation of the VSSI$_D$ MCV chart is demonstrated with the dataset from Khatun, *et al.* [37]. The data deal with the measurements of a spring, i.e. spring inner diameter (X_1) and spring elasticity (X_2). The Phase-I data consist of m = 10 samples, each with $n_0 = 5$. Table 4 presents the Phase-I sample means, sample variances, and sample covariances. The Phase-I in-control sample MCV is assumed based on the root mean square method, expressed in Eq. (5) as $\sqrt{\frac{1}{10}\sum_{i=1}^{10}\hat{\gamma}_i^2} = 0.001042$. Consequently, the LCL of the SH$_D$ MCV chart [18] can be computed using Eq. (8) as follows:

$$\text{LCL}=F_{\hat{\gamma}}^{-1}\left(0.0027 \middle| 5, 2, \frac{5}{0.001042^2}\right) = 0.000129 \tag{19}$$

for the upward SH$_D$ MCV chart. Here, α is set as 0.0027 to satisfy ATS$_0$=370. Figure 2 shows the SH$_D$ MCV chart. The Phase-I process is declared in-control as all the $\hat{\gamma}_i$ are plotted above the LCL of the SH$_D$ MCV chart.

Suppose that a practitioner wants to find an unexpected decrease in MCV shifts of the process for the Phase-II process monitoring. The VSSI$_D$ MCV chart was designed to compute the ATS$_1$ for the downward MCV shift $\tau = 0.7$. The optimal parameter $(n_1, n_2, h_1, h_2, \alpha', \alpha)$ combination for the VSSI$_D$ MCV chart is obtained using the aforementioned optimization procedure in Section 3 as $(n_1, n_2, h_1, h_2, \alpha', \alpha)$ = (4, 31, 0.1, 1.0346, 0.0396, 0.0027), subject to ATS$_0$=370. Subsequently, the LCL = 0.0001 and LWL = 0.0009 can be obtained using Eq. (8) and Eq. (10). Note that the pair (n_1, h_2) is first considered since the initial probabilities obtained from Eq. (14a) and Eq. (14b) show that $b_1 = 0.75 > b_2 = 0.25$ for the VSSI$_D$ MCV chart. Thus, State 1 is used as the initial state.

Table 1 Optimal parameters (n_1, n_2, h_2, α') of VSSI$_D$ MCV chart for minimizing ATS$_1$ and EATS$_1$ when $p \in \{2.3\}$, $n_0 \in \{5,10\}$, $\gamma_0 \in \{0.1, 0.3, 0.5\}$, $h_1 = 0.1$, $\tau \in \{0.5, 0.6, 0.7, 0.8, 0.9\}$, $(\tau_{max}, \tau_{min}) = [0.5,1)$ and ATS$_0$=370.

τ	$p = 2$			$p = 3$		
	$\gamma_0 = 0$	$\gamma_0 = 0.3$	$\gamma_0 = 0.5$	$\gamma_0 = 0.1$	$\gamma_0 = 0.3$	$\gamma_0 = 0.5$
			$n_0 = 5$			
0.5	3, 10, 1.360, 0.2876	3, 9, 1.450, 0.3351	3, 10, 1.360, 0.2876	4, 12, 1.129, 0.1274	4, 12, 1.129, 0.1274	4, 13, 1.113, 0.1135
0.6	3, 16, 1.164, 0.1561	3, 16, 1.164, 0.1561	3, 18, 1.139, 0.1357	4, 20, 1.060, 0.0650	4, 21, 1.056, 0.0614	4, 23, 1.050, 0.0552
0.7	3, 31, 1.069, 0.0739	3, 31, 1.069, 0.0739	3, 31, 1.069, 0.0739	4, 31, 1.035, 0.0396	4, 27, 1.041, 0.0461	4, 31, 1.035, 0.0396
0.8	3, 31, 1.069, 0.0739	3, 31, 1.069, 0.0739	3, 31, 1.069, 0.0739	4, 31, 1.035, 0.0396	4, 31, 1.035, 0.0396	4, 31, 1.035, 0.0396
0.9	3, 6, 2.800, 0.6676	3, 6, 2.800, 0.6676	3, 6, 2.800, 0.6676	4, 6, 1.900, 0.5013	4, 6, 1.900, 0.5013	4, 6, 1.900, 0.5013
			$n_0 = 10$			
0.5	6, 17, 1.514, 0.3654	6, 16, 1.600, 0.4016	6, 17, 1.514, 0.3654	7, 17, 1.386, 0.3019	6, 15, 1.720, 0.4459	7, 17, 1.386, 0.3019
0.6	6, 19, 1.400, 0.3096	4, 17, 1.771, 0.4630	5, 19, 1.500, 0.3589	6, 19, 1.400, 0.3096	4, 15, 2.080, 0.5467	6, 20, 1.360, 0.2876
0.7	5, 29, 1.237, 0.2105	4, 22, 1.450, 0.3351	4, 31, 1.257, 0.2243	5, 29, 1.237, 0.2105	5, 23, 1.346, 0.2797	5, 31, 1.214, 0.1945
0.8	3, 11, 7.300, 0.8753	3, 13, 3.100, 0.7008	3, 11, 7.300, 0.8753	4, 11, 6.400, 0.8575	4, 13, 2.800, 0.6676	4, 11, 6.400, 0.8575
0.9	3, 11, 7.300, 0.8753	3, 13, 3.100, 0.7008	3, 11, 7.300, 0.8753	4, 11, 6.400, 0.8575	4, 13, 2.800, 0.6676	4, 11, 6.400, 0.8575

(τ_{max}, τ_{min})	$p = 2$			$p = 3$		
	$\gamma_0 = 0$	$\gamma_0 = 0.3$	$\gamma_0 = 0.5$	$\gamma_0 = 0.1$	$\gamma_0 = 0.3$	$\gamma_0 = 0.5$
			$n_0 = 5$			
[0.5, 1)	3, 6, 2.800, 0.6676	3, 6, 2.800, 0.6676	3, 6, 2.800, 0.6676	4, 6, 1.900, 0.5013	4, 6, 1.900, 0.5013	4, 6, 1.900, 0.5013
			$n_0 = 10$			
[0.5, 1)	3, 11, 7.300, 0.8753	3, 11, 7.300, 0.8753	3, 11, 7.300, 0.8753	4, 11, 6.400, 0.8575	4, 11, 6.400, 0.8575	4, 11, 6.400, 0.8575

Table 2 ATS$_1$ and EATS$_1$ values for VSSI$_D$ MCV and SH$_D$ MCV charts when $p = 2$, $n_0 \in \{5,10\}$, $\gamma_0 \in \{0.1, 0.3, 0.5\}$, $h_1 = 0.1$, $\tau \in \{0.5, 0.6, 0.7, 0.8, 0.9\}$, , $(\tau_{max}, \tau_{min}) = [0.5,1)$ and ATS$_0$ = 370.

τ	ATS$_1$											
	$n_0 = 5$											
	VSSI$_D$ MCV			VSS$_D$ MCV			VSI$_D$ MCV			SH$_D$ MCV		
	$\gamma_0 = 0.1$	$\gamma_0 = 0.3$	$\gamma_0 = 0.5$	$\gamma_0 = 0.1$	$\gamma_0 = 0.3$	$\gamma_0 = 0.5$	$\gamma_0 = 0.1$	$\gamma_0 = 0.3$	$\gamma_0 = 0.5$	$\gamma_0 = 0.1$	$\gamma_0 = 0.3$	$\gamma_0 = 0.5$
0.5	2.56	2.60	2.84	4.69	4.72	5.11	6.18	6.29	6.86	33.43	52.15	55.84
0.6	5.41	5.59	6.70	7.11	7.98	8.98	12.11	12.77	14.71	64.03	87.72	93.57
0.7	15.52	15.68	19.89	17.71	18.12	22.74	32.55	33.33	38.87	103.67	135.30	142.81
0.8	80.80	81.93	98.25	83.49	87.80	104.09	85.43	86.90	96.18	129.98	198.12	204.75
0.9	203.13	204.42	214.12	227.32	256.49	266.05	205.96	208.42	224.61	237.24	277.14	282.74
	$n_0 = 10$											
0.5	1.18	1.19	1.22	2.02	2.03	2.13	1.46	1.51	1.62	5.28	5.88	7.08
0.6	1.58	1.62	1.71	2.74	2.93	3.23	2.47	2.52	2.83	14.50	15.94	18.55
0.7	3.12	3.18	3.78	5.86	6.23	7.46	5.31	6.03	7.39	36.56	39.28	44.45
0.8	16.70	17.28	20.17	26.15	27.34	33.90	23.11	24.43	30.01	80.33	86.08	96.26
0.9	88.68	90.43	98.72	147.58	154.59	166.49	105.16	107.41	118.35	187.53	190.22	197.42
(τ_{max}, τ_{min})	EATS$_1$											
	$n_0 = 5$											
	VSSI$_D$ MCV			VSS$_D$ MCV			VSI$_D$ MCV			SH$_D$ MCV		
	$\gamma_0 = 0.1$	$\gamma_0 = 0.3$	$\gamma_0 = 0.5$	$\gamma_0 = 0.1$	$\gamma_0 = 0.3$	$\gamma_0 = 0.5$	$\gamma_0 = 0.1$	$\gamma_0 = 0.3$	$\gamma_0 = 0.5$	$\gamma_0 = 0.1$	$\gamma_0 = 0.3$	$\gamma_0 = 0.5$
[0.5, 1)	100.69	102.10	107.49	108.33	120.71	127.45	104.02	104.31	112.16	118.30	179.07	185.68
	$n_0 = 10$											
[0.5, 1)	52.60	53.40	55.85	72.23	73.41	77.03	56.99	57.96	62.46	94.43	98.25	104.91

Table 3 ATS_1 and $EATS_1$ values for $VSSI_D$ MCV and SH_D MCV charts when $p = 3$, $n_0 \in \{5,10\}$, $\gamma_0 \in \{0.1, 0.3, 0.5\}$, $h_1 = 0.1$, $\tau \in \{0.5, 0.6, 0.7, 0.8, 0.9\}$, , $(\tau_{max}, \tau_{min}) = [0.5,1)$ and $ATS_0 = 370$.

τ	ATS_1											
	$n_0 = 5$											
	$VSSI_D$ MCV			VSS_D MCV			VSI_D MCV			SH_D MCV		
	$\gamma_0 = 0.1$	$\gamma_0 = 0.3$	$\gamma_0 = 0.5$	$\gamma_0 = 0.1$	$\gamma_0 = 0.3$	$\gamma_0 = 0.5$	$\gamma_0 = 0.1$	$\gamma_0 = 0.3$	$\gamma_0 = 0.5$	$\gamma_0 = 0.1$	$\gamma_0 = 0.3$	$\gamma_0 = 0.5$
0.5	5.24	5.42	6.36	7.64	7.82	8.67	10.27	11.97	13.31	93.38	96.66	103.00
0.6	12.79	13.29	15.97	14.94	15.10	17.61	23.13	25.34	29.32	135.17	139.23	146.12
0.7	37.64	38.57	46.98	38.49	39.54	49.32	56.23	58.83	67.10	183.46	186.39	194.52
0.8	142.73	145.04	164.27	145.31	148.52	167.58	120.84	124.45	134.79	237.73	241.67	248.88
0.9	259.18	260.56	267.85	289.12	293.75	300.02	263.32	268.24	274.36	302.76	304.71	309.54
	$n_0 = 10$											
0.5	1.24	1.27	1.30	2.19	2.29	2.33	1.62	1.74	1.89	8.22	8.46	9.88
0.6	1.76	1.93	1.95	2.87	3.28	3.62	2.88	3.07	3.48	20.33	21.05	24.26
0.7	3.78	3.94	4.70	6.92	7.07	8.58	7.05	7.73	9.54	44.02	48.60	54.47
0.8	21.43	23.21	25.92	30.75	32.21	40.05	29.08	30.27	36.83	101.49	103.33	111.62
0.9	102.47	110.39	113.17	157.08	169.74	181.76	112.68	119.34	130.58	202.16	203.71	210.63

τ_{max}, τ_{min}	$EATS_1$											
	$n_0 = 5$											
	$VSSI_D$ MCV			VSS_D MCV			VSI_D MCV			SH_D MCV		
	$\gamma_0 = 0.1$	$\gamma_0 = 0.3$	$\gamma_0 = 0.5$	$\gamma_0 = 0.1$	$\gamma_0 = 0.3$	$\gamma_0 = 0.5$	$\gamma_0 = 0.1$	$\gamma_0 = 0.3$	$\gamma_0 = 0.5$	$\gamma_0 = 0.1$	$\gamma_0 = 0.3$	$\gamma_0 = 0.5$
[0.5, 1)	131.83	132.74	150.09	134.82	136.86	155.54	151.76	152.72	159.73	216.66	220.08	226.32
	$n_0 = 10$											
[0.5, 1)	57.47	58.39	61.04	76.82	77.83	81.77	61.74	62.52	67.38	203.86	206.56	213.28

Table 4 Phase-I data.

Sample number (i)	Sample means		Sample variances and covariances			
	Spring inner diameter ($\bar{X}_{1i}$)	Spring elasticity ($\bar{X}_{2i}$)	S_{1i}^2	S_{2i}^2	S_{12i}	$\hat{\gamma}_i$
1	28.24	45.93	0.0044	0.0484	-0.0127	0.0008
2	28.33	45.88	0.0118	0.0029	-0.0022	0.0009
3	28.31	45.69	0.0016	0.0169	-0.0036	0.0007
4	28.26	45.89	0.0006	0.0118	0.0007	0.0008
5	28.31	45.84	0.0011	0.0222	-0.0003	0.0011
6	28.28	45.89	0.0034	0.0134	-0.0063	0.0004
7	28.33	45.78	0.0040	0.0071	-0.0036	0.0008
8	28.31	45.78	0.0025	0.0081	0.0009	0.0014
9	28.32	45.80	0.0027	0.0492	0.0070	0.0017
10	28.32	45.80	0.0009	0.0077	0.0017	0.0010

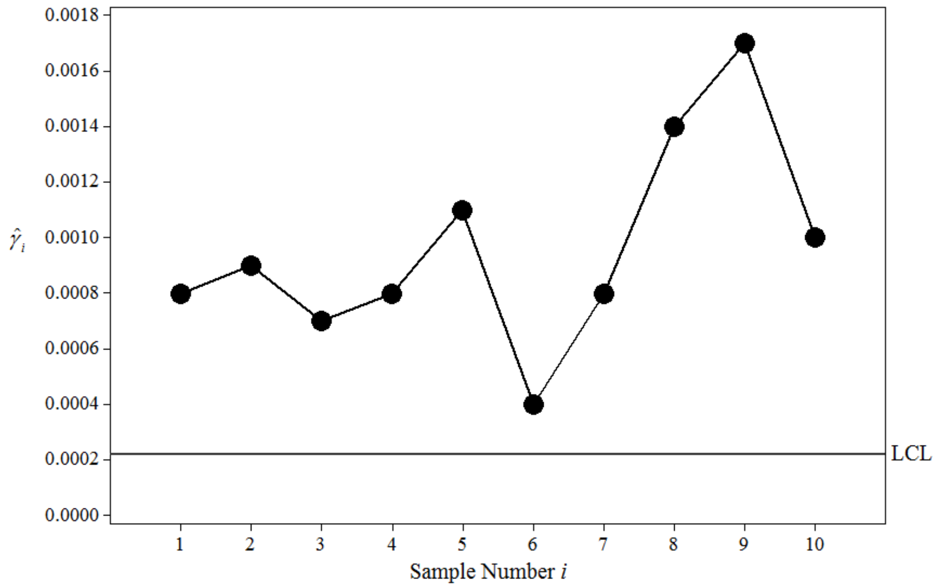

Figure 2 SH$_D$ MCV chart for the Phase-I process.

Figure 3 presents the VSSI$_D$ MCV chart. In Table 5, the VSSI$_D$ MCV chart does not detect any out-of-control signal. However, the processing time has been shortened to 6.61 hours (or equivalently 6 hours 37 minutes) instead of 10 hours. Conversely, when the out-of-control signals are detected, the practitioner should look into the underlying process for identifying the assignable cause(s). After that, immediate corrective action should be taken to revert the out-of-control process to the normal condition.

Table 5 Phase-II data.

Phase-II data									
Sample number (i)	**Sample means**		**Sample variances and covariances**			$\hat{\gamma}_i$	n_1 (or n_1)	h_1 (or h_2)	**Cumulative time (in hours)**
	Spring inner diameter ($\bar{X}_{1i}$)	Spring elasticity ($\bar{X}_{2i}$)	S_{1i}^2	S_{2i}^2	S_{12i}				
1	28.27	45.83	0.0075	0.0695	-0.0207	0.0009	4	1.0346	1.0346
2	28.30	45.83	0.0018	0.0136	-0.0044	0.0004	4	1.0346	2.0692
3	28.34	45.75	0.0004	0.0154	0.0010	0.0007	31	0.1	2.1692
4	28.29	45.84	0.0055	0.0291	-0.0099	0.0013	31	0.1	2.2692
5	28.25	45.92	0.0013	0.0472	0.0012	0.0013	4	1.0346	3.3038
6	28.30	45.80	0.0032	0.0160	-0.0066	0.0004	4	1.0346	4.3384
7	28.32	45.89	0.0061	0.0122	-0.0023	0.0016	31	0.1	4.4384
8	28.25	45.88	0.0003	0.0193	-0.0017	0.0004	4	1.0346	5.4730
9	28.27	45.84	0.0074	0.0111	0.0020	0.0021	31	0.1	5.5730
10	28.25	45.95	0.0052	0.0337	-0.0119	0.0007	4	1.0346	6.6076

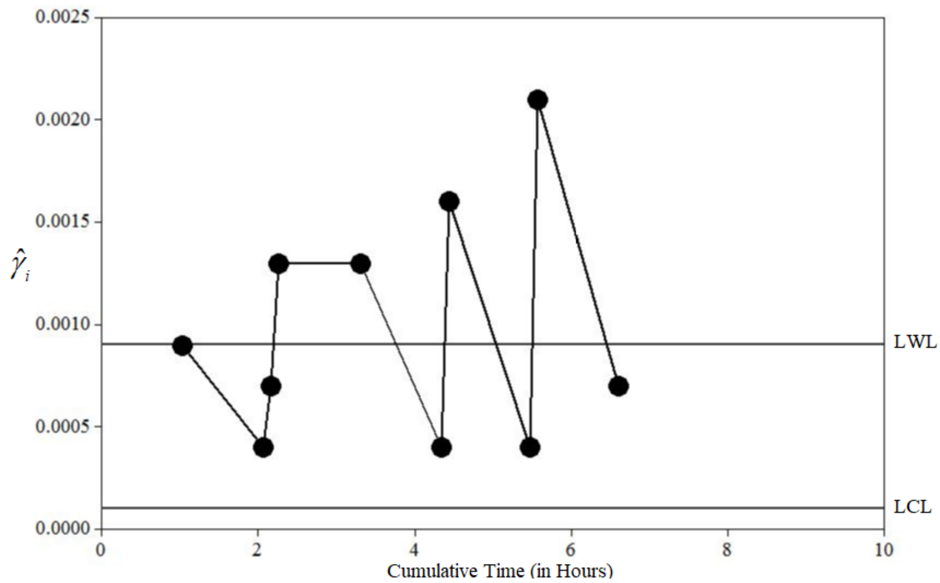

Figure 3 VSSID MCV chart for the Phase-II process.

6 Conclusion

A one-sided VSSI$_D$ MCV chart was proposed to monitor the downward MCV shifts in terms of the ATS$_1$ and EATS$_1$ criteria. In the existing literature, the existing VSSI$_D$ MCV chart only monitors upward MCV shifts. In certain scenarios, the detection of downward MCV shifts is very important as it shows process improvement. This research circumvents this problem by proposing a one-sided VSSI$_D$ MCV chart. Additionally, the proposed one-sided chart is also able to circumvent biased ATS and EATS performances. The VSSI$_D$ MCV chart outperforms the SH$_D$ MCV chart in detecting small and moderate downward MCV shifts in terms of the ATS$_1$ and EATS$_1$ criteria. The application of the proposed chart was illustrated using an example with a real dataset. The one-sided VSSI$_D$ MCV chart is flexible in allows the n and h parameters to be varied by referring to the current process quality. This flexibility is able to increase the effectiveness of the process monitoring system and save production costs at the same time. In future research, the design of the one-sided VSSI$_D$ MCV chart can be further extended with measurement errors as well as estimated process parameters.

Acknowledgements

This work was funded by the Kementerian Pendidikan Malaysia, Fundamental Research Grant Scheme [grant number 203.PMGT.6711755]. Special thanks are extended to the School of Management, Universiti Sains Malaysia, Malaysia.

References

[1] Djauhari, M.A., *A Unifying Concept of X Chart and X-Bar Chart When Subgroup Sizes Are Equal*, Journal of Mathematical and Fundamental Sciences, **30**(1), pp. 27-30, 1998.

[2] Chen, G., Cheng, S.W. & Xie, H., *A New EWMA Control Chart for Monitoring Both Location and Dispersion,* Quality Technology & Quantitative Management, **1**(2), pp. 217-231, 2004.

[3] Wang, W., *Maintenance Models Based On the Np Control Charts with Respect to The Sampling Interval,* Jouirnal of the Operational Research Society, **62**(1), pp. 124-133, 2011.

[4] Chong, N.L., Khoo, M.B.C., Haridy, S. & Shamsuzzaman, M., *A Multiattribute Cumulative Sum-np Chart*, Stat, **8**(1), e239, 2019.

[5] Singh, G. & Singh, K., *Video Frame and Region Duplication Forgery Detection Based On Correlation Coefficient and Coefficient of Variation*, Multimedia Tools and Applications, **78**(9), pp. 11527-11562, 2019.

[6] Salmanpour, S., Monfared, H. & Omranpour, H., *Solving Robot Planning Problem by Using a New Elitist Multi-Objective IWD Algorithm Based On Coefficient of Variation*, Soft Computing, **21**(11), pp. 3063-3079, 2017.

[7] Lengler, J. & Steger, A., *Note On the Coefficient of Variations of Neuronal Spike Trains,* Biological Cybernetics, **111**(3-4), pp. 229-235, 2017.

[8] Zhou, Z., Kizil, M., Chen, Z. & Chen, J., *A New Approach for Selecting Best Development Face Ventilation Mode Based On G1-Coefficient of*

Variation Method, Journal of Central South University, **25**(10), pp. 2462-2471, 2018.

[9] Ye, J., Feng, P., Xu, C., Ma, Y. & Huang, S., *A Novel Approach for Chatter Online Monitoring Using Coefficient of Variation in Machining Process,* The International Journal of Advanced Manufacturing Technology, **96**(1-4), pp. 287-297, 2018.

[10] Centore P., *The Coefficient of Variation as A Measure of Spectrophotometric Repeatability*, Color Research and Application, **41**(6), pp. 571-579, 2016.

[11] Ushigome, E., Fukui, M., Hamaguchi, M., Senmaru, T., Sakabe, K., Tanaka, M., Yamazaki, M., Hasegawa, G. & Nakamura, N., *The Coefficient Variation of Home Blood Pressure Is a Novel Factor Associated with Macroalbuminuria in Type 2 Diabetes Mellitus*, Hypertension Research, **34**, pp. 1271-1275, 2011.

[12] Romano, F.L., Ambrosano, G.M.B., Magnani, M.B.B.A. & Nouer, D.F., *Analysis of The Coefficient of Variation in Shear and Tensile Bond Strength Tests*, Journal of Applied Oral Science, **13**(3), pp. 243-246, 2005.

[13] Kang, C., Lee, M., Seong, Y. & Hawkins, D., *A Control Chart for The Coefficient of Variation,* Journal of Quality Technology, **39**(2), pp. 151-158, 2007.

[14] Khaw, K.W., Khoo, M.B.C., Yeong, W.C. & Wu, Z., *Monitoring The Coefficient of Variation Using a Variable Sample Size and Sampling Interval Control Chart,* Communications in Statistics - Simulation and Computation, **46**(7), pp. 5772-5794, 2017.

[15] Yeong W.C., Lim S.L., Khoo M.B.C. & Castagliola P., *Monitoring The Coefficient of Variation Using a Variable Parameters Chart,* Quality Engineering, **30**(2), pp. 212-235, 2018.

[16] Khaw, K.W. & Chew, X.Y., *A Re-Evaluation of the Run Rules Control Chart for Monitoring the Coefficient of Variation,* Statistics, Optimization & Information Computing, **7**(4), pp. 716-730, 2019.

[17] Lim, S.L., Yeong, W.C., Khoo, M.B.C., Chong, Z.L. & Khaw, K.W., *An Alternative Design for The Variable Sample Size Coefficient of Variation Chart Based On the Median Run Length and Expected Median Run Length*, International Journal of Industrial Engineering: Theory, Applications and Practice, **26**(2), pp. 199-220, 2019.

[18] Yeong W.C., Khoo M.B.C., Teoh W.L. & Castagliola P., *A Control Chart for The Multivariate Coefficient of Variation*, Quality and Reliability Engineering International, **32**(3), pp. 1213-1225, 2016.

[19] Khaw K.W., Khoo M.B.C., Castagliola P. & Rahim M.A., *New Adaptive Control Charts for Monitoring the Multivariate Coefficient of Variation,* Computers & Industrial Engineering, **126**, pp. 595-610, 2018.

[20] Khaw K.W., Chew X.Y., Yeong W.C. & Lim S.L., *Optimal Design of the Synthetic Control Chart for Monitoring the Multivariate Coefficient of Variation,* Chemometrics and Intelligent Laboratory Systems, **186**, pp. 33-40, 2019.

[21] Chew, X.Y., Khaw, K.W. & Yeong, W.C., The Efficiency of Run Rules Schemes for The Multivariate Coefficient of Variation: A Markov Chain Approach, Journal of Applied Statistics, 47(3), pp. 460-480, 2020.

[22] Chew, X.Y., Khoo, M.B.C., Khaw, K.W., Yeong, W.C. & Chong, Z.L., *A Proposed Variable Parameter Control Chart for Monitoring the Multivariate Coefficient of Variation*, Quality and Reliability Engineering International, **35**(7), pp. 2442-2461, 2019.

[23] Giner-Bosch, V., Tran, K.P., Castagliola, P. & Khoo, M.B.C., *An EWMA Control Chart for The Multivariate Coefficient of Variation.* Quality and Reliability Engineering International, **35**(6), pp. 1515-1541, 2019.

[24] Haq, A. & Khoo, M.B.C., *New Adaptive EWMA Control Charts for Monitoring Univariate and Multivariate Coefficient of Variation,* Computers & Industrial Engineering, **131**, pp. 28-40, 2019.

[25] Epprecht, E., Costa, A.F.B. & Mendes, F.C.T., *Adaptive Control Charts for Attributes*, IIE Transactions, **35**(6), pp. 567-582, 2003.

[26] Deheshvar, A., Shams, H., Jamali, F. & Movahedmanesh, Z., *A Novel Adaptive Control Chart with Variable Sample Size, Sampling Interval and Control Limits: A Three Stage Variable Parameters (TSVP)*, International Journal of Business and Management, **8**(2), pp. 38-49, 2013.

[27] Prabhu, S.S, Montgomery & D.C., Runger, G.C., *A Combined Adaptive Sample Size and Sampling Interval $\bar{X}$ Control Scheme,* Journal of Quality Technology, **26**(3), pp. 164-176, 1994.

[28] Saha, S., Khoo, M.B.C., Lee, M.H. & Haq, A., *A Variable Sample Size and Sampling Interval Control Chart for Monitoring the Process Mean Using Auxiliary Information*, Quality Technology & Quantitative Management, **16**(4), pp. 389-406, 2019.

[29] Kosztyan Z.T. & Katona, A.I., *Risk-Based X-Bar Chart with Variable Sample Size and Sampling Interval,* Computers & Industrial Engineering, **120**, pp. 308-319, 2018.

[30] Khoo, M.B.C., See, M.Y., Chong, N.L. & Teoh, W.L., *An Improved Variable Sample Size and Sampling Interval S Control Chart,* Quality and Reliability Engineering International, **35**(1), pp. 392-404, 2019.

[31] Cheng, X. & Wang, F., *VSSI Median Control Chart with Estimated Parameters and Measurement Errors*, Quality and Reliability Engineering International, **34**(5), pp. 867-881, 2018.

[32] Aparisi, F. & Haro, C.L., *A Comparison of T^2 Control Charts with Variable Sampling Schemes as Opposed to MEWMA Chart*, International Journal of Production Research, **41**(10), pp. 2169-2182, 2003.

[33] Voinov, V.G. & Nikulin, M.S. *Unbiased Estimator and Their Applications, Multivariate* Case, **2**, Kluwer: Dordrecht, 1996.

[34] Chong, Z.L., Khoo, M.B.C., Teoh, W.L., You, H.W. & Castagliola, P., *Optimal Design of The Side-Sensitive Modified Group Runs (SSMGR)* $\bar{X}$ *Chart When Process Parameters Are Estimated*, Quality and Reliability Engineering International, **35**(1), pp. 246-262, 2019.

[35] Siddall J.N., Probabilistic Engineering Design-Principles and Applications, Marcel Dekker: New York, 1983.

[36] Castagliola, P., Celano, G. & Psarakis, S., *Monitoring The Coefficient of Variation Using EWMA Charts*, Journal of Quality Technology, **43**(3), pp. 249-265, 2011.

[37] Khatun, M., Khoo, M.B.C., Lee, M.H. & Castagliola, P., *One-Sided Control Charts for Monitoring the Multivariate Coefficient of Variation in Short Production Runs*, Transactions of the Institute of Measurement and Control, **41**(6), pp. 1712-1728, 2019.